http://dx.doi.org/10.21611/qirt.2012.186

QIRT 2012

11th International Conference on
Quantitative InfraRed Thermography

Line-focus Beam-scan Time-domain Active Thermography with External Control

by T. Hoshimiya*, J. Hoshimiya and M.Tsuda

*Dept. of Electronic Engineering, Tohoku Gakuin University, 13-1, Chuo 1, Tagajyo, 985-8537, Japan,
tpth@tjcc.tohoku-gakuin.ac.jp

Abstract

An active thermographic imaging system was constructed, in which a linearly-focused cw laser beam was scanned toward a direction perpendicular to the beam covering whole surface of a specimen with a simulated internal defect. A real-time response of the thermotracer was recorded to construct both thermal image time-variation of the specimen and the temperature waveform at each individual image pixel. External I/O control for triggering of both thermotracer recording and laser irradiation was achieved. Calculated data agreed well with the experimental data.

1. Introduction

Active-thermography or photothermal radiometry has become more and more important as a nondestructive inspection (NDI) tool in industrial applications. Continuous wave (cw) [1], pulse [2], or moving heat source [3] methods are dominant technique for them. However, the extremely fast movement of heat source, such as 100m/sec is required for inspection of metals or materials with high-thermal conductivity [3].

In this study, the thermographic instrumentation system, in which a line-focus laser beam scans over specimen surface with external I/O control, was designed, constructed and demonstrated. A thermotracer real-time response at an individual image pixel was compared with the theoretical calculation.

2. Theory

2.1. Model

The model for calculation is shown in Fig. 1. A line-shaped heat source, which is generated with a linearly focused laser or light beam and aligned parallel to the y-axis, moves toward the +x-direction with a constant velocity v. The coordinate of the line-heat source $x_s(t)$ is described as

$$x_s(t) = -x_0 + v \cdot t \qquad (1)$$

A generated thermal wave, which has a cylindrical wave front, is diffused into a solid specimen under study. The specimen with a thickness d and length $2x_0$ is assumed to have a slit-shaped internal defect (with width y_0 and depth d-σ) as shown in Fig. 2. The upper boundary of the internal defect is set to be located at the depth σ.

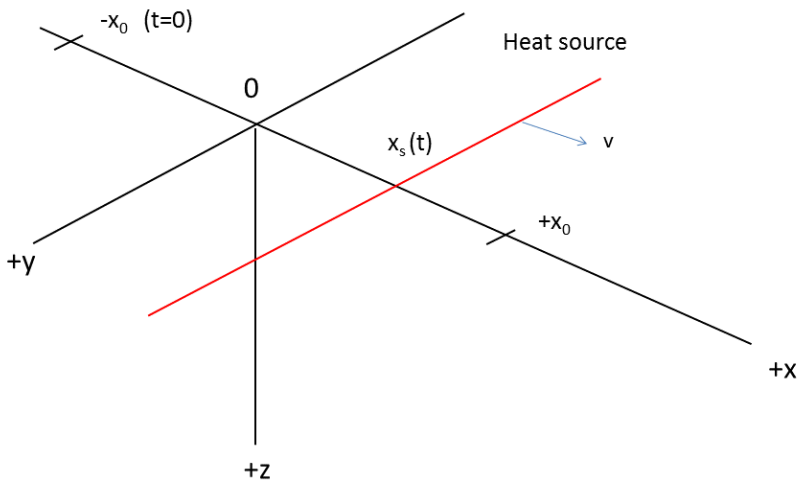

Fig. 1. *Model Heat-source arrangement.*

http://dx.doi.org/10.21611/qirt.2012.186

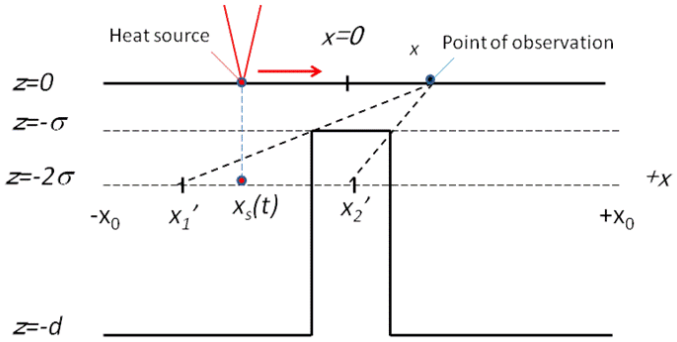

Fig. 2. *Cross-sectional view of the specimen.*

Image technique [4] shows that an imaginary heat source moving in the range between x1'<x<x2' at the depth z=-2σ can reach to the observation point at the coordinate x on the specimen surface (z=0) as shown in the figure.

Integration of a space-temporal Green's function [5] for a moving heat-source (x'=vt', z'=0);

$$T(x,0,z,t) = \frac{q}{8\rho c(\pi\kappa)^{3/2}}\int_0^t dt' \int_{-\infty}^{\infty} dy' \int_{-\infty}^{\infty} G(x,0,zt;vt',y',0,t')dz'$$

$$= \frac{q}{4\pi\kappa\rho c}\int_0^t \frac{\exp[-\frac{(x^2+z^2}{4\kappa(t-t')}]}{t-t'}\,dt' \qquad (2)$$

where the quantity q and κ represent amount of heat and thermal diffusivity, respectively.

After integration over line-heat source, at center (y=0) specimen surface (z=0), it was rewritten with an incomplete Gamma function [6] as two components; for surface diffusion component as;

$$T_0(x,0,0,t) = \frac{q}{4\pi\kappa\rho c}\cdot\Gamma(0,\frac{(x-x_s)^2}{4\kappa t}) \qquad (3)$$

and the internal reflected component as;

$$T_1((x,0,z,t) = \frac{q}{8\rho c(\pi\kappa)^{3/2}}\int_0^t dt' \int_{-\infty}^{\infty} dy' \int_{-\infty}^{\infty} G(x,0,zt;vt',y',-2\sigma,t')dz'$$

$$= \begin{cases} \frac{q}{4\pi\kappa\rho c}\int_{t_1'}^{t_2'} \frac{\exp\left[-\frac{(x^2+z^2}{4\kappa(t-t')}\right]}{t-t'}\,dt' & for \quad t > t_2' \\ \frac{q}{4\pi\kappa\rho c}\int_0^t \frac{\exp[-\frac{(x^2+z^2}{4\kappa(t-t')}]}{t-t'}\,dt' & for \quad t_1' < t < t_2' \end{cases} \qquad (4)$$

In the above expression times t_1' and t_2' correspond to the times the laser beam reached at the edges x_1' and x_2' at the imaginary plane (z=-2σ), respectively.

3. Experimental apparatus and specimens

3.1. Apparatus

The experimental setup is shown in Fig. 3. A second harmonics of diode-pumped Nd-YAG laser (DPSSL) with wavelength of 532nm was used as optical source. Its beam was expanded with a beam-expander with a magnification x10. For translation of a laser beam, linear-motor slider was used. A collimated beam was incident into a right-angle prism and a plano-convex cylindrical lens both attached to a moving slider. The beam was focused with a cylindrical lens on the specimen surface with a width of about 250 μm, length of 30mm, and the power of 145mW.A thermal image was observed by a thermo-tracer (NEC San-ei, TH 9100) with a temperature resolution of 0.06K. The thermal image was recorded by a PC connected with an IEEE 1394 bus. The real-time (30 flames/sec) thermal response was recorded by a PC. Experimental condition was as follows: laser power was 145 mW. Stage moving speed was 1 mm/sec, and the resolution of the thermotracer was 320×240 pixel.

To reduce noise in obtained temperature waveforms, averaging procedure is favorable. To align starting timing of the recording, external I/O box was introduced as shown in the figure.

3.2. Specimens

Specimens with various thermal properties were used as a trial. They were polyoxymethylene plastic (delrin), brass and 18 Cr-8 Ni alloy stainless steel (SUS304). The specimens studied in detail were made of stainless steel (SUS304), and they have a cuboid shape with a size of 25mmx 40mm x4mm^t. The thermal properties of the material are as follows:

density ρ = 7920 [kg/m3],
specific heat c = 0.499 [kJ/ (kg ·K)]
thermal conductivity λ = 16.0 [W/ (m·K)].

As simulated undersurface defects, rectangular slits with a width (y_0) of 3, 5 and 10mm and depths (σ) of 0.5, 1.0, and 1.5 mm were fabricated inside of the specimen, and focused laser beam was aligned to the slit. The specimen surface was coated by black-body paint with an absorbance of 0.94.

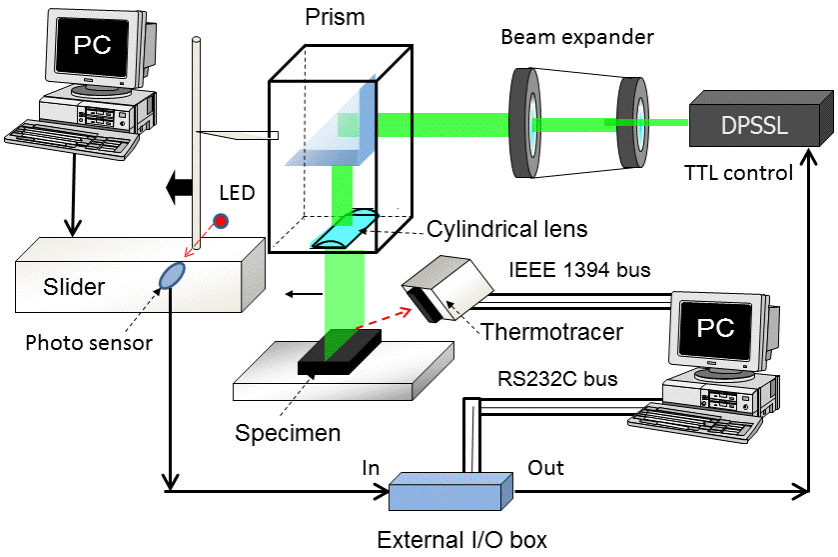

Fig. 3 *Basic experimental arrangement*

4. Experimental results

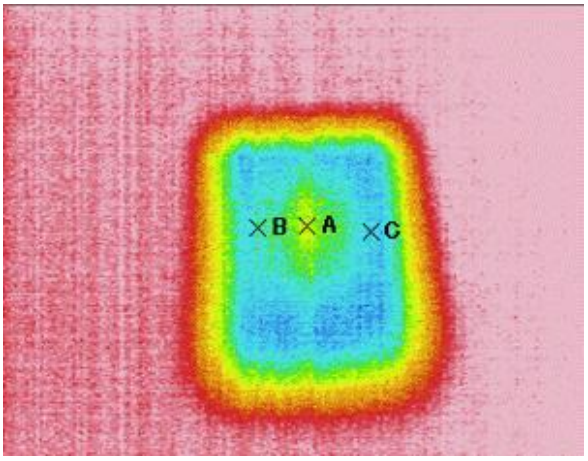

Fig. 4 Thermal image obtained for the case depth 0.5mm, width 10mm.

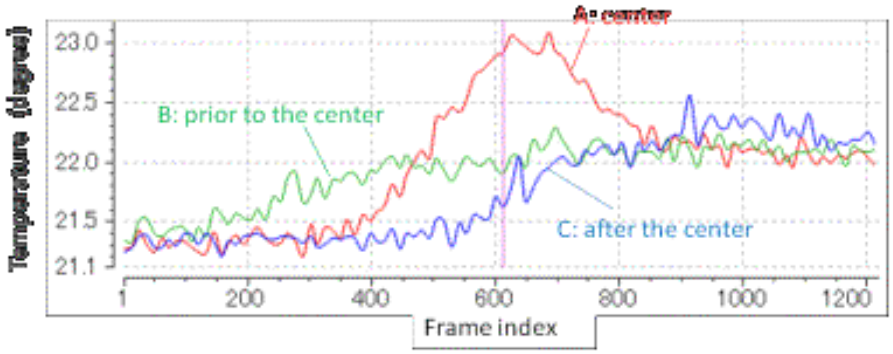

Fig. 5 Temperature trend signals observed at A (center), B (prior to the center) and C (after the center) shown in Fig. 4

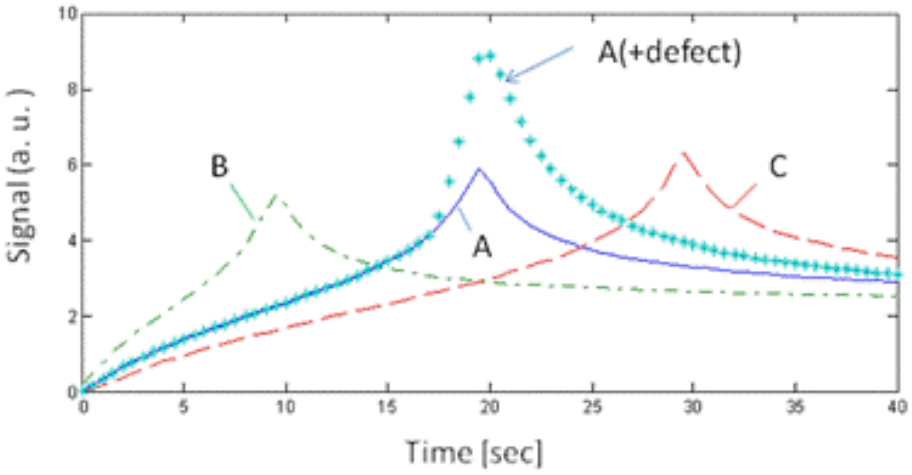

Fig. 6 Calculated temperature waveform

Figures 4 and 5 show thermographic image and its temporal variation of the surface temperature waveform of a SUS304 specimen with an internal defect (depth 0.5mm, width 10mm), respectively. The points A, B and C represent center, prior to the center, after the center, respectively. B and C both located with distances of 5mm apart from the center. The frame index (0-1200) is converted to time sequence (0-40 sec).

For comparison, theoretical waveforms corresponding to the observed points A, B, and C were calculated with equations (3) and (4), and the results were shown in Fig. 6.

The experimentally obtained waveforms agreed well with theoretically calculated waveforms shown in Figure 4, in which thermal response without internal defect (A, B, C) and with defect were shown.

Using a software “ir-motion”, timings for individual recording of the thermal image were adjusted with a LED-photo-sensor pair so that the accumulation of the recorded waveform data were stored with a PC. The averaging of data stored with a CSV (Excel) form reduces random temperature fluctuation on the waveform. The averaging of N-times measurements approximately improved S/N by the factor of square root N.

5. Conclusions

In this paper, an active thermographic imaging system with external I/O control was constructed. Experimental results show thermographic response signal increase caused by the reflection of heat flow at the internal defect boundary.

The main contributions of the present detection scheme are as follows:

1) Time-domain photothermal radiometric inspection technique using line-focus moving heat source was proposed and demonstrated.

2) Theoretical analysis including the reflection of thermal wave at the internal defect boundary was carried out and agreed with experimental data qualitatively.

3) This scheme has an ability to detect internal defects with a good spatial resolution, and has an advantage to adjust moving velocity change to specimens and to utilize time-domain control by laser light pulse width or frequency modulation for materials with high thermal conductivities such as metals.

REFERENCES

[1] Breitenstein O and M. Langenkamp, *“Lock-in Thermography”,* Springer, Berlin, 2003.

[2] Favro L. D., Jin H. J., Kuo P. K., Thomas R. L., and Wang Y. X., “Real-time Thermal Wave Tomography”, Photoacoustic and Photothermal Phenomena III (Ed. By D. Bicanic), Springer, Berlin, pp. 519-521, 1992.

[3] Favro L.D. , Kuo P. K. and Thomas R. L., “Real-time Thermal Wave Imaging”, Nondestructive Evaluation (NDE), Progress in Photoacoustic and Photothermal Phenomena (Ed. by A. Mandelis), pp.23-51,1994.

[4] Thomas R.L .et.al., “Subsurface flaw detection in metals by photoacoustic microscopy”, J. Appl. Phys., vol. 51, pp.1152-1156, 1980.

[5] Carlslaw H.S. and Jaeger J. C.,"Conduction of Heat in Solids", Oxford, 1959.

[6] Abramowitz, M. and Stegun, I. A. (Eds.). “Handbook of Mathematical Functions with Formulas, Graphs, and Mathematical Tables” , Dover, 1972.